

## Understanding about Image-guided Detection of Prostate Cancer

Hwun-Jae Lee<sup>1\*</sup>

Received: 20 October 2022 / Accepted: 25 November 2022 / Published online: 30 December 2022

©The Author(s) 2022

**Abstract** - The prostate is both an accessory gland of the male reproductive system and a muscle-driven mechanical switch between urination and ejaculation. Anatomically, the prostate is found below the bladder, with the urethra passing through it. Prostate cancer (PCa) is the second-most prevalent cancer and the fifth leading cause of cancer-specific mortality in male, worldwide. Currently, the only sure way to confirm prostate cancer is through a prostate biopsy. Rapid technological advances over the past few years have enabled the mainstream use of prostate imaging for the clinical management of prostate cancer. In biopsy for the diagnosis of prostate cancer, prostate imaging technology is mobilized to extract tissue from the exact area. Ultrasound imaging, MRI, and PET imaging methods are used for prostate imaging methods. Although each image has its own characteristics, the recent trend is the fusion image method that uses each other's strengths. There is currently no technology that can fully meet the clinical requirements of speed and high precision at the same time at low cost.

The development of a biopsy framework that is inexpensive, easy to use, and has minimal clinical overhead seems necessary. This requires the implementation of new image registration and visualization approaches and the establishment of a research platform for rapid bench-to-bed conversion.

**Key word:** Prostate cancer, US-guided Biopsy, MR imaging-guided biopsy, PET imaging-guided biopsy, Multimodal Imaging-guided biopsy

### I. Introduction

The prostate is a walnut-sized male gonads. The prostate gland secretes a slightly alkaline milky liquid, which is a prostate-specific antigen that makes up semen, and produces and secretes a dilute alkaline liquid that accounts for 20-30% of the ejaculate. This fluid, along with sperm and seminal vesicle secretions, constitutes 50 to 75% of semen. The alkalinity of semen helps to neutralize the acidity of the vaginal canal and increases the lifespan of sperm. The smallest structural component of the prostate gland are surrounded by a basement membrane that separates the secretory epithelial cells from surrounding structures<sup>[1]</sup>. A risk factor directly related to the development of prostate cancer is age. Prostate cancer is very rare in people under the age of 40, and

---

H. J. Lee(✉)<sup>1\*</sup>

<sup>1\*</sup>YUHS-KRIBB Medical Convergence Research Institute, Yonsei University Health System, Seoul 03722, Republic of Korea

Department of Radiology, College of Medicine, Yonsei University, Seoul 03722, Republic of Korea

increases rapidly in proportion to age after the age of 50<sup>[2]</sup>. Animal fat in meat is known to cause prostate cancer by affecting the secretion and function of sex hormones. Early-stage prostate cancer is often asymptomatic. Despite extensive efforts, finding a serum prostate-specific antigen(PSA) cutoff that can reliably indicate the presence of cancer or the need for a biopsy has been challenging. This is because serum PSA levels are gland specific biomarkers rather than cancer specific. That is, it is expressed not only in hyperplastic cells of the prostate, especially in benign prostatic hyperplasia(BPH), but also in cancer cells<sup>[3]</sup>. Biomarkers need to find additional avenues to improve early detection, risk stratification and disease monitoring for prostate cancer patients. The clinical management of prostate cancer is one of the most controversial areas in medicine, with no consensus on the need for cancer screening, the choice of diagnostic tests for pretreatment evaluation, and the necessity and appropriateness of treatment for all stages of the disease. Currently, the only definitive way to confirm prostate cancer is through a prostate biopsy<sup>[4]</sup>. A prostate biopsy is the removal of a small sample of prostate tissue to test for signs of prostate cancer<sup>[5]</sup>. Rapid technological advances over the past few years have enabled the mainstream use of prostate imaging for the clinical management of prostate cancer<sup>[5]</sup>. Evolving techniques of real-time ultrasound elastography(RTE) and contrast-enhanced ultrasound(CEUS) are being investigated to better detect and improve the yield by allowing “targeted” biopsies<sup>[6]</sup>. Last decade has witnessed rapid developments in magnetic resonance imaging(MRI) for improved management of prostate cancer. In addition to the anatomical information, it is capable of providing functional information through diffusion-weighted imaging(DWI), magnetic resonance spectroscopy(MRS), and dynamic contrast-enhanced (DCE) MRI. Multi-parametric

MRI has the potential to exclude a significant cancer in the majority of cases. Inclusion of MRI before prostatic biopsy can reduce the invasiveness of the procedure by limiting the number of cores needed to make a diagnosis and support watchful waiting in others<sup>[7]</sup>. It is made possible by targeted biopsies as opposed to random. With the availability of minimally invasive therapeutic modalities like high-intensity focused ultrasound(HIFU) and interstitial laser therapy, detecting early cancer is even more relevant today<sup>[7]</sup>. [<sup>18</sup>F]--fluorodeoxyglucose positron emission tomography/computed tomography (<sup>18</sup>FDG PET/CT) has no role in the initial evaluation of prostate cancer. Choline PET has been recently found to be more useful. Fluoride-PET has a higher sensitivity and resolution than a conventional radionuclide bone scan in detecting skeletal metastases<sup>[8]</sup>. In this paper, we discuss and evaluate the important evolutionary role of multimodal imaging for biopsy guidelines aimed at early detection of prostate cancer or recurrence after treatment.

## II. Prostate cancer

The prostate is both an accessory gland of the male reproductive system and a muscle-driven mechanical switch between urination and ejaculation. Anatomically, the prostate is found below the bladder, with the urethra passing through it<sup>[9]</sup>.

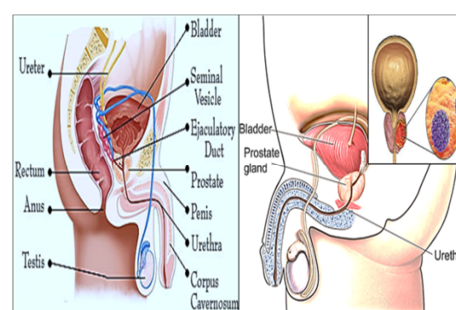


Figure 1. Prostate anatomy and tumor

It is described in gross anatomy as consisting of lobes and in microanatomy by zone. It is surrounded

by an elastic, fibromuscular capsule and contains glandular tissue as well as connective tissue. The prostate glands produce and contain fluid that forms part of semen, the substance emitted during ejaculation as part of the male sexual response. This prostatic fluid is slightly alkaline, milky or white in appearance. The alkalinity of semen helps neutralize the acidity of the vaginal tract, prolonging the lifespan of sperm. The prostatic fluid is expelled in the first part of ejaculate, together with most of the sperm, because of the action of smooth muscle tissue within the prostate. In comparison with the few spermatozoa expelled together with mainly seminal vesicular fluid, those in prostatic fluid have better motility, longer survival, and better protection of genetic material. Disorders of the prostate include enlargement, inflammation, infection, and cancer. The prostate is a gland of the male reproductive system. In adults, it is about the size of a walnut<sup>[10]</sup>, and has an average weight of about 11 grams, usually ranging between 7 and 16 grams<sup>[11]</sup>. The prostate is located in the pelvis. It sits below the urinary bladder and surrounds the urethra. The part of the urethra passing through it is called the prostatic urethra, which joins with the two ejaculatory ducts<sup>[10]</sup>. The prostate is covered in a surface called the prostatic capsule or prostatic fascia<sup>[12]</sup>. The internal structure of the prostate has been described using both lobes and zones<sup>[11]</sup>. Because of the variation in descriptions and definitions of lobes, the zone classification is used more predominantly<sup>[10]</sup>. The prostate has been described as consisting of three or four zones<sup>[10][13]</sup>. Zones are more typically able to be seen on histology, or in medical imaging, such as ultrasound or MRI<sup>[11]</sup>.

The zones are:

1. Peripheral zone (PZ) :70%(adult gland)

The back of the gland that surrounds the distal urethra and lies beneath the capsule. About 70–

80% of prostatic cancers originate from this zone of the gland<sup>[12]</sup>.

2. Central zone (CZ) :20%(adult gland)

This zone surrounds the ejaculatory ducts.<sup>[11]</sup> The central zone accounts for roughly 2.5% of prostate cancers; these cancers tend to be more aggressive and more likely to invade the seminal vesicles<sup>[12]</sup>.

3. Transition zone (TZ) :5%(adult gland)

The transition zone surrounds the proximal urethra.<sup>[11]</sup> 10–20% of prostate cancers originate in this zone. It is the region of the prostate gland that grows throughout life and causes the disease of benign prostatic enlargement<sup>[12]</sup>

4. Anterior fibro-muscular zone

This area, not always considered a zone<sup>[12]</sup>, is usually devoid of glandular components and composed only, as its name suggests, of muscle and fibrous tissue<sup>[12]</sup>.

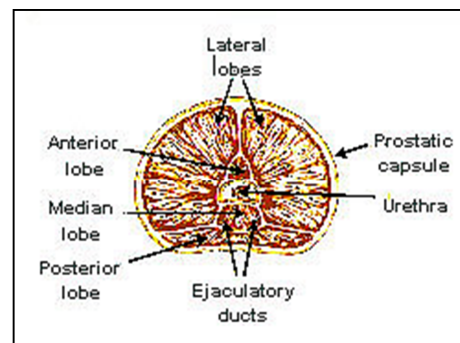


Figure 2. Zone of the prostate gland

The prostate consists of glandular and connective tissue<sup>[12]</sup>. Tall column-shaped cells form the lining (the epithelium) of the glands<sup>[12]</sup>. These form one layer or may be pseudostratified<sup>[12]</sup>. The epithelium is highly variable and areas of low cuboidal or flat cells can also be present, with transitional epithelium in the outer regions of the longer ducts<sup>[13]</sup>. The glands are formed as many follicles, which in drain into canals and subsequently 12–20 main ducts, these in turn drain into the urethra as it passes through the prostate<sup>[12]</sup>. There are also a small amount of flat

cells, which sit next to the basement membranes of glands, and act as stem cells<sup>[12]</sup>. The connective tissue of the prostate is made up of fibrous tissue and smooth muscle<sup>[12]</sup>. The fibrous tissue separates the gland into lobules<sup>[12]</sup>. It also sits between the glands and is composed of randomly orientated smooth-muscle bundles that are continuous with the bladder<sup>[10]</sup>. Over time, thickened secretions called corpora amylacea accumulate in the gland<sup>[12]</sup>.



Figure 3. Micrograph of benign prostatic glands with corpora amylacea<sup>[12]</sup>.

The prostate secretes fluid which becomes part of semen. Semen is the fluid emitted (ejaculated) by males during the sexual response<sup>[14]</sup>. When sperm is emitted, it is transmitted from the vas deferens into the male urethra via the ejaculatory ducts, which lie within the prostate gland<sup>[14]</sup>. Ejaculation is the expulsion of semen from the urethra<sup>[14]</sup>. Semen is moved into the urethra following contractions of the smooth muscle of the vas deferens and seminal vesicles, following stimulation, primarily of the glans penis. Stimulation sends nerve signals via the internal pudendal nerves to the upper lumbar spine; the nerve signals causing contraction act via the hypogastric nerves<sup>[14]</sup>. After traveling into the urethra, the seminal fluid is ejaculated by contraction of the bulbocavernosus muscle<sup>[14]</sup>. The secretions of the prostate include proteolytic enzymes, prostatic acid phosphatase, fibrinolysin, zinc, and prostate-specific antigen<sup>[12]</sup>. Together with the secretions from the seminal vesicles, these form the major fluid part of

semen<sup>[14]</sup>. The prostate's changes of shape, which facilitate the mechanical switch between urination and ejaculation, are mainly driven by the two longitudinal muscle systems running along the prostatic urethra. These are the urethral dilator (musculus dilatator urethrae) on the urethra's front side, which contracts during urination and thereby shortens and tilts the prostate in its vertical dimension thus widening the prostatic section of the urethral tube<sup>[12]</sup>, and the muscle switching the urethra into the ejaculatory state (musculus ejaculatorius) on its backside<sup>[13]</sup>. Cancer starts when cells in the body begin to grow out of control. Cells in nearly any part of the body can become cancer cells, and can then spread to other areas of the body. Prostate cancer begins when cells in the prostate gland start to grow out of control. Almost all prostate cancers are adenocarcinomas. These cancers develop from the gland cells (the cells that make the prostate fluid that is added to the semen). Other types of cancer that can start in the prostate include<sup>[15]</sup>:

- (1) Small cell carcinomas
- (2) Neuroendocrine tumors
- (3) Transitional cell carcinomas
- (4) Sarcomas

Some prostate cancers grow and spread quickly, but most grow slowly. In fact, autopsy studies show that many older men who died of other causes also had prostate cancer that never affected them during their lives. In many cases, neither they nor their doctors even knew they had it<sup>[15]</sup>.

### III. Imaging modalities

Imaging has now become an essential option for detecting and localizing prostate cancer. Current major modalities for image-guided diagnosis of prostate cancer include methods such as ultrasound-

based imaging, multiparameter MRI, multiparameter MRI-ultrasound fusion imaging, and PET imaging. The choice of imaging modality is determined by the biological behavior of the underlying tumor.

### 1. Microbubbles Ultrasound-based imaging

Nanobubbles (NBs), as novel ultrasound contrast agents (UCAs), have attracted increasing attention in the field of molecular ultrasound imaging for tumors. However, the preparation of uniform-sized NBs is considered to be controversial, and poor tumor selectivity in *in vivo* imaging has been reported. HengliYang et al fabricated uniform nano-sized NBs ( $478.2 \pm 29.7$  nm with polydispersity index of  $0.164 \pm 0.044$ ,  $n = 3$ ) using a thin-film hydration method by controlling the thickness of phospholipid films. And then conjugated the NBs with Affibody molecules to produce nano-sized UCAs referred to as NB-Affibody with specific affinity to human epidermal growth factor receptor type 2 (HER2)-overexpressing tumors. NB-Affibody presented good ultrasound enhancement, demonstrating a peak intensity of  $104.5 \pm 2.1$  dB under ultrasound contrast scanning. *Ex vivo* experiments further confirmed that the NB-Affibody conjugates were capable of targeting HER2-expressing tumor cells *in vivo* with high affinity. The newly prepared nano-sized NB-Affibody conjugates were observed to be novel targeted UCAs for efficient and safe specific molecular imaging and may have potential applications in early cancer quantitative diagnosis and targeted therapy in the future<sup>[17]</sup>.

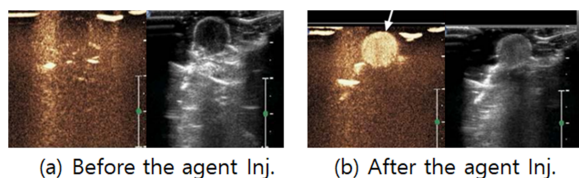


Figure 4. Results of a study on microbubbles<sup>[18]</sup>.

### 2. Computer-aided US image analysis

To objectify the interpretation of prostate, ultrasound images were processed by a computer-based image analysis system (IAS). The IAS “tissue descriptors” are not dependent on the gray scale. Transrectal ultrasound (TRUS) images, results of the IAS and pathologic whole mounts (PWM), were correlated in an attempt to define the efficiency of the IAS in differentiating carcinoma from normal tissue of the prostate. Using the closely correlated TRUS and PWM slices, a restrictive setting (high specificity) of the IAS yielded rates of 90% (true positive), 10% (false negative) and 5% (false positive). Using a less restrictive setting (higher sensitivity), rates of 100% (true positive), 10% (false negative) and 12% (false positive) were noted. These encouraging results were obtained from the peripheral zone of the prostate. However, the clinical false-positive and false-negative rates for IAS have not yet been determined<sup>[18]</sup>.

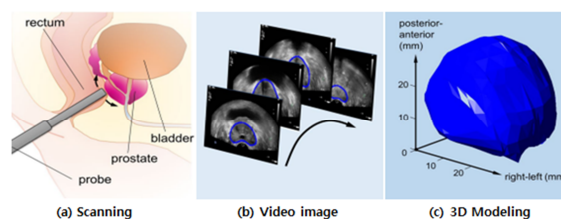


Figure 5. Example of *in vivo* 3D reconstruction of the prostate based on a 2D US video<sup>[19]</sup>

### 3. Prostate HistoScanning

Prostate HistoScanning™ (PHS) is an ultrasound-based tissue characterisation technique that has previously shown encouraging results in the detection of clinically significant prostate cancer. The present study reports on the open ‘unblinded’ phase of a European multicentre study. The prospective ‘blind’ phase is currently in progress and will determine the value of PHS in a robust fashion overcoming many of the biases inherent in evaluating

prostate imaging<sup>[20]</sup>.

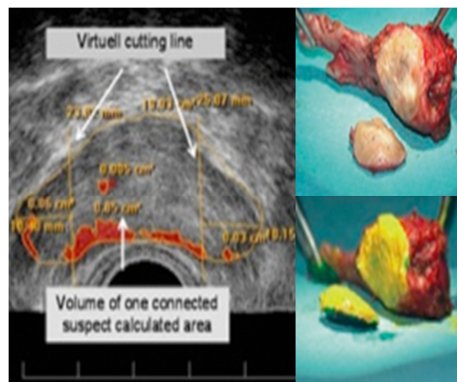


Figure 5. Accuracy of HistoScanning™ for the prediction of a negative surgical margin in patients undergoing radical prostatectomy<sup>[22]</sup>

#### 4. Transrectal US

Estimation of prostate gland volume with transrectal ultrasound may provide important information in the evaluation of benign and malignant prostatic diseases. To determine the most accurate means of volume estimation 150 patients underwent transrectal ultrasound with 15 separate methods of volume estimation. All patients underwent subsequent radical prostatectomy or cystoprostatectomy. Prostate specimen weights were compared with the results of each volume estimation method. Step-section planimetry, previously assumed to be the most accurate means of volume measurement, exhibited a Pearson correlation coefficient of 0.93. The elliptical volume, widely used as an alternative to planimetry, demonstrated a correlation coefficient of 0.90. The most accurate method to estimate prostate weight ( $r = 0.94$ ) was a variation of the prolate spheroid formula, expressed as  $\pi/6$  (transverse dimension)<sup>2</sup> (anteroposterior dimension). When different volume ranges were considered, this prolate spheroid formula provided the closest estimate of weight in glands of less than 40 gm. and those in the 40 to 80 gm. range. The most accurate method to estimate prostates weighing greater than 80 gm. was the formula  $\pi/6$  (transverse dimension)<sup>[23]</sup>.

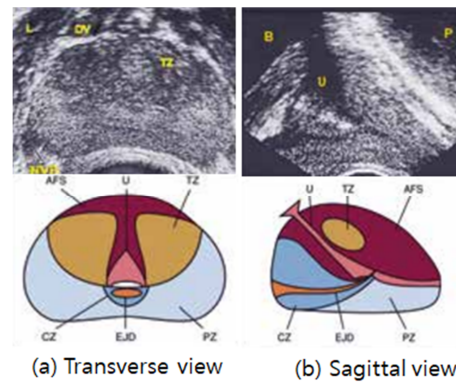


Figure 6. Normal prostate ultrasound images with zonal anatomy Normal prostate ultrasound images (top) with diagrams (bottom) at approximately the level of the verumontanum demonstrating zonal anatomy. A, Transverse view. B, Sagittal view. AFS, anterior fibromuscular stroma; CZ, central zone; DV, dorsal vascular complex; EJD, ejaculatory ducts; NVB, neurovascular bundle; L, levator muscles; PZ, peripheral zone; TZ, transition zone; U, urethra. [Source: Campbell Walsh Urology, permission see page 44.]

#### 5. Doppler US

To determine the role of color Doppler imaging (CDI) in diagnosis of prostate cancer. Transrectal ultrasound (TRUS) and CDI were performed in 456 patients with possible prostate cancer. Of these patients, 158 underwent prostate biopsy, and these formed the study group. The frequency of malignancy was 47% (75 of 158). Of 136 TRUS-positive cases, 72 were malignant and 64 benign. Of 84 CDI-positive cases, 65 were malignant and 19 benign ( $\chi^2 = 12.18, P < .001$ ). Thirteen percent of histopathologically proven cases (10 of 75) were normal at CDI. TRUS alone had a sensitivity of 96% and a positive predictive value (PPV) of 0.53. The addition of CDI increased the PPV to 0.77 but reduced the sensitivity to 87%. In only one case out of 158 did CDI suggest the diagnosis of malignancy independently of TRUS. CDI improves the PPV of TRUS but appears to have little additional value over TRUS alone in diagnosis of prostate cancer<sup>[24]</sup>.

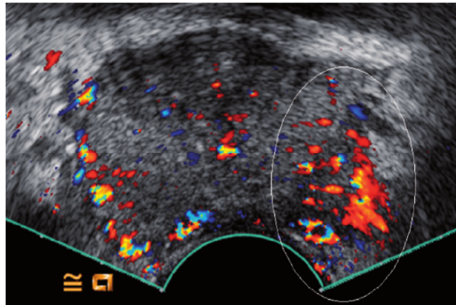


Figure 7. Corresponding contrast-enhanced colour Doppler US showing clearly more enhancement of the left side (white ellipsoid) <sup>[25]</sup>.

## 6. Contrast enhanced US

Ultrasound imaging of the prostate is commonly used to assess the size of the gland and for needle placement during systematic biopsy. Ultrasound evaluation of prostate cancer is limited by difficulty in distinguishing benign from malignant tissue. Although Doppler techniques may provide some improvement in the detection of prostate cancer, targeted biopsy based on conventional ultrasound with Doppler is not sufficient to replace systematic biopsy. Contrast-enhanced ultrasound imaging techniques that employ microbubble contrast agents represent an innovative approach to imaging of the neovascularity associated with prostate cancer. This review describes the application of contrast-enhanced ultrasound to improve detection and assessment of prostate cancer <sup>[26]</sup>.

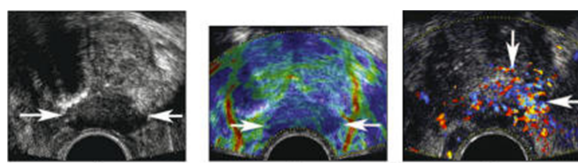


Figure 8. An 80-year-old man biopsy cores demonstration Gleason 9 and 10 cancer in the left midgland: A. Conventional gray scale image shows a hypoechoic mass extending exophytically from the prostate (arrows). The hypoechoic appearance is the classic description for prostate cancer. B. Real-time elastography shows reduced tissue elasticity (darker blue color) in the region of the mass (arrows). C. Color Doppler shows increased flow within and

around the mass (arrows) <sup>[26]</sup>

## 7. Real time elastography

Palpation of organs is one of the oldest clinical examination techniques, for instance, if you think of the palpation of the breast or the digital rectal examination of the prostate, where hard palpable regions are suspicious for cancer. This is the basic principle of real-time elastography, an ultrasound technique, which is able to visualize tissue elasticity. Since prostate cancer features an increased stiffness due to the higher cell and vessel density than the normal surrounding tissue, real-time elastography has been used for several years for prostate cancer detection. This review introduces the different techniques of ultrasound elastography and furthermore summarises its limitations and potentials. Histopathological evaluation of systematic biopsy (SB) cores is used to confirm or rule out cancer. In SB, the conventional transrectal ultrasound (TRUS) is primary utilized for biopsy guidance and not for cancer detection, because suspicious hypoechoic areas represent cancer in only 9–53% of cases in the grey-scale technique <sup>[27]</sup>. Despite the low specificity of PSA testing and the low sensitivity of SB, these techniques remain the standard of care for PCa diagnosis, mainly because of the high availability and low costs <sup>[28]</sup>. Nevertheless, on the one hand, this strategy misses significant PCa in a high percentage of patients and, on the other hand, detects many insignificant PCa, which leads to overdiagnosis and overtherapy <sup>[29]</sup>. Because of encouraging technical innovations and developments in prostate imaging, it is now possible to visualize PCa with high sensitivity <sup>[30]</sup>. Besides PCa localization, modern imaging modalities are capable of providing information about tumor volume, local staging, and cancer aggressiveness, which may be helpful for choosing

the most appropriate therapy<sup>[31]</sup>.

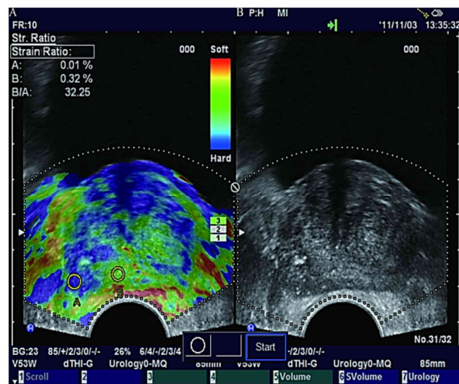


Figure 9. Transrectal real-time tissue elastography targeted biopsy coupled with peak strain index improves the detection of clinically important prostate cancer<sup>[32]</sup>

## 8. Shear wave elastography

This prospective study was to evaluate shear wave elastography (SWE) in the detection of prostate cancer (PC). Patients scheduled for a transrectal ultrasound (TRUS) biopsy of the prostate because of elevated prostate-specific antigen levels or abnormal digital rectal examination result underwent a standard TRUS and SWE. A second TRUS examination and sextant biopsy by a second physician blinded to SWE results was then performed. Pathologic result was reviewed, and sensitivity, specificity, negative predictive value (NPV), and positive predictive value (PPV) were calculated. A total of 53 patients (318 sextants) participated in the study. Mean age was 64.2 years (range, 53–79 years). A total of 26 foci of PC were detected in 11 patients (20.7%). On the basis of the receiver operating characteristic curve, a value of 37 kPa was used as the cutoff between benign and malignant. This produced a sensitivity of 96.2% (25/26), a specificity of 96.2% (281/292), a PPV of 69.4% (25/36), and an NPV of 99.6% (281/282). Six (55%) of 11 false-positive samples were secondary to benign calcifications. The Young modulus of PC ranged from 30 to 110 kPa (mean [SD], 58.0 [20.7] kPa). At the patient level, if a cutoff

of 40 kPa was used, all PCs would have been detected, and the positive biopsy rate would be 11 (50%) of 22 compared to 11 (20.8%) of 53 without SWE—a 140% increase in the positive biopsy rate. Shear wave elastography has a high sensitivity, specificity, PPV, and NPV for the detection of PC. With a high PPV, patients with elevated prostate-specific antigen levels or abnormal results in the digital rectal examination and negative SWE may not require biopsy. This could significantly reduce the negative biopsy rate in PC detection<sup>[33]</sup>.

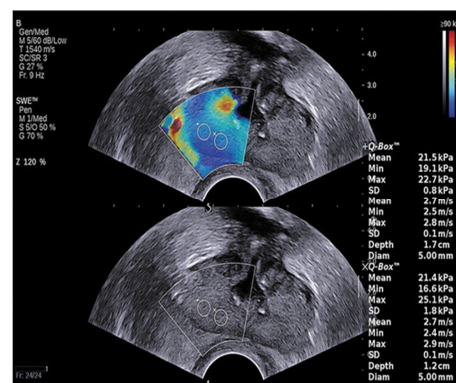


Figure 10. Diagnostic value of transrectal shear wave elastography for prostate cancer detection in peripheral zone<sup>[33]</sup>

## 9. Acoustic radiation force impulse imaging

It has been challenging for clinicians using current imaging modalities to visualize internal structures and detect lesions inside human prostates. Lack of contrast among prostatic tissues and high false positive or negative detection rates of prostate lesions have limited the use of current imaging modalities in the diagnosis of prostate cancer. In this study, acoustic radiation force impulse (ARFI) imaging is introduced to visualize the anatomical and abnormal structures in freshly excised human prostates. A modified Siemens Antares ultrasound scanner (Siemens Medical Solutions USA Inc., Malvern, PA) and a Siemens VF10-5 linear array were used to acquire ARFI images. The transducer was attached to a three-dimensional (3-D) translation stage, which

was programmed to automate volumetric data acquisition. A depth dependent gain (DDG) method was developed and applied to 3-D ARFI datasets to compensate for the displacement gradients associated with spatially varying radiation force magnitudes as a function of depth. Nine human prostate specimens were collected and imaged immediately after surgical excision. Prostate anatomical structures such as seminal vesicles, ejaculatory ducts, peripheral zone, central zone, transition zone and verumontanum were visualized with high spatial resolution and in good agreement with McNeal's zonal anatomy. The characteristic appearance of prostate pathologies, such as prostate cancerous lesions, benign prostatic hyperplasia, calcified tissues and atrophy were identified in ARFI images based upon correlation with the corresponding histologic slides. This study demonstrates that ARFI imaging can be used to visualize internal structures and detecting suspicious lesions in the prostate and appears promising for image guidance of prostate biopsy<sup>[34]</sup>.

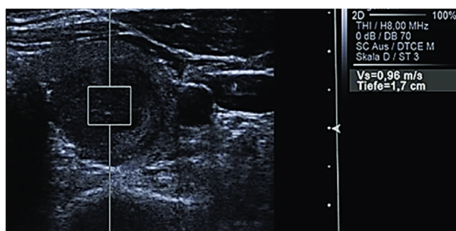


Figure 11. Acoustic radiation force-based elasticity imaging<sup>[35]</sup>

## 10. Multiparameter US

Soft tissue needle insertion characterization has been a focus of many medical and biomedical recent studies. In this study the constrained prostate soft tissue deformation through a finite element model is evaluated. The study considers a sensitivity analysis of the target reaching error with respect to the mechanical, insertion and anatomical parameters in

presence of the kinematics constraint on the tissue. The needle insertion into the soft tissue is simulated using the proposed Finite Element Method (FEM). Based on acquired results, the insertion of needle induces a considerable rotation of the prostate tissue due to its specific kinematics and support structure. Such rotation can increase the sensitivity of the error to mechanical properties of the tissue especially to the Poisson ratio. It is shown that even minor changes in Poisson ratio (4%) leads to large target reaching errors (9 fold)<sup>[30]</sup>.

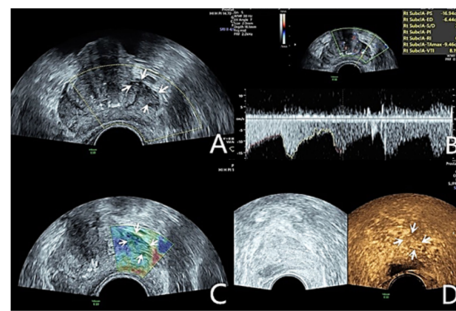


Figure 12. Multiparameter US for prostate cancer<sup>[37]</sup>

## 11. MR Imaging

This presents a state-of-the-art technique for multiparametric magnetic resonance (MR) imaging of prostate cancer. The technical requirements and clinical indications for the use of multiparameter MR imaging in the detection, localization, characterization, staging, biopsy guidance, and active surveillance of prostate cancer are discussed. Although the reported accuracies of individual and combined multiparameter MR imaging techniques vary for various clinical prostate cancer indications, multiparameter MR imaging of the prostate has shown promising results and is of additional value for prostate cancer localization and local staging. The combination of technical approaches (field strength, sequence, use of intrarectal coils) and multiparameter MR imaging techniques to be used for specific clinical indications remains a challenge. Due

to the current lack of guidelines, suggestions for a general minimal protocol for multiparameter MR imaging of the prostate are presented based on the literature and the authors' experiences. A computer program capable of evaluating the various components of a multiparameter MR imaging examination in one view needs to be developed. In this way, integrated interpretation of anatomical and functional MR imaging modalities is possible in multiparameter MR imaging examinations. Professional radiologist training and experience are essential to correctly interpret multiparameter prostate MR imaging findings. Obtaining fast, cost-effective, easy, and reproducible prostate cancer diagnosis from increasingly complex multivariate MR imaging data requires assistive technologies such as computer-aided diagnosis<sup>[38]</sup>.

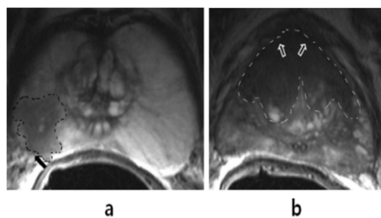


Figure 13. Axial T2-weighted turbo spin-echo MR images (repetition time msec/echo time msec, 4260/99; flip angle 120°) of prostate cancer<sup>[38]</sup>.

Figure 13 (a) is at level of midprostate to apex, a low-signal-intensity. The lesion is present on the right side of the prostate, within the high signal intensity of the peripheral zone (outline), with signs of minimal capsular invasion (arrow). At prostatectomy, this lesion, which was suspicious for prostate cancer, corresponded to stage T3a (extracapsular extension of 5 mm), Gleason score 7 (4+3) prostate cancer. Figure 13 (b) is at midprostate level, a homogeneous low signal intensity area in the ventral transition zone is seen (outline), with loss of visibility of healthy BPH structures (“charcoal sign”). Invasion of anterior fibromuscular stroma at the ventral prostate can be seen (arrows). This lesion was

suspicious for transition zone cancer. At prostatectomy, stage T2c, Gleason score 6 (2+4) prostate cancer was found<sup>[38]</sup>.

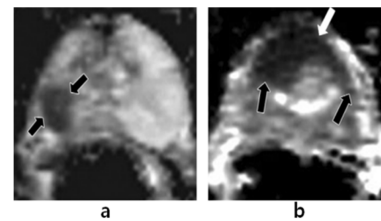


Figure 14. DW imaging of prostate cancer. Axial ADC maps (2400/81; b = 0, 50, 500 and 800 sec/mm<sup>2</sup>) obtained at midprostate level in same patients as in Figure 1a (a) and 1b (b). (a) Lesion with low ADC (mean ADC = 0.8 3 10 2 3 mm<sup>2</sup>/sec), is suspicious for cancer in right peripheral zone (arrows)<sup>[38]</sup>.

This indicates intermediate to high cancer aggressiveness. At prostatectomy, the lesion was determined to be stage T3a, Gleason score 7 (4+3) prostate cancer. (b) Comma-shaped area with low ADC (mean ADC = 0.6 3 10 2 3 mm<sup>2</sup>/sec) is seen in ventral transition zone (arrows). This indicates intermediate to high cancer aggressiveness. At prostatectomy, lesion was determined to be stage T2c, Gleason score 6 (2+4) prostate cancer.

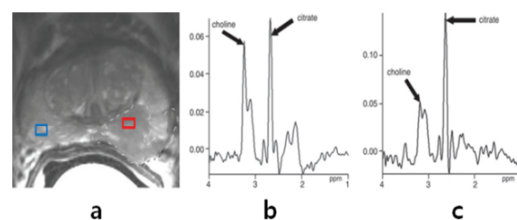


Figure 15. MR spectroscopic imaging in a 70-year-old man (same as in Fig 18) with a PSA level of 12 ng/mL and well-differentiated prostate cancer<sup>[38]</sup>.

Figure 15(a) is axial T2-weighted turbo spin-echo MR image (4260/99; flip angle, 120°) shows stage T3a prostate cancer. Radical prostatectomy revealed a solitary Gleason score 7 (3+4) adenocarcinoma with extraprostatic extension. Red voxel has been placed in low-signal-intensity lesion in left peripheral zone, which is suspicious for cancer; The blue voxel has been placed in benign-appearing region in right peripheral zone. (b) is MR spectrum (750/145; flip

angle,  $90^\circ$ ) from red voxel shows choline peak that is increased relative to citrate peak. The choline plus creatine-to-citrate ratio, calculated from the integrals of the spectral peaks from choline, creatine, and citrate, is 0.80, which is suspicious for prostate cancer. (c) is MR spectrum ( $750/145$ ; flip angle,  $90^\circ$ ) from blue voxel demonstrates low choline peak and high citrate peak, consistent with benign peripheral zone tissue. The choline plus creatine-to-citrate ratio is 0.32.

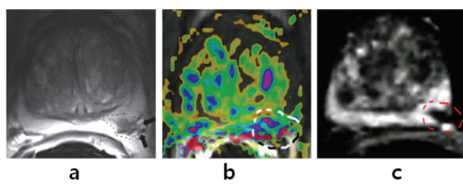


Figure 16. Multiparametric MR imaging in a 69-year-old man undergoing active surveillance of Gleason score 6 (3+3) prostate cancer, found in 5% of the volume of one (left-sided) of nine systematic random biopsy core specimens. The patient had a PSA level of 6.7 ng/mL, PSA density of 0.9 ng/mL/mL, and clinical stage T2 disease. Multiparametric MR imaging findings obtained with an endorectal coil were suspect for stage T3a cancer in the left peripheral zone at the midprostate level. DW imaging findings indicated tumor intermediate to highly aggressive tumor at the same location<sup>[38]</sup>.

Figure 16 (a) is Axial T2-weighted turbo spin-echo MR image obtained with endorectal coil ( $4260/99$ ; flip angle,  $120^\circ$ ) at midprostate level shows small area of lower signal intensity in left peripheral zone (outline) with signs of extracapsular extension (arrows). (b) is Axial MR image with superimposed Ktrans parametric map ( $38/1.35$ ; flip angle,  $14^\circ$ ; same level as a and b) at the same level as (a). Early enhancement occurs in multiple areas. The region suspicious for tumor is also enhanced (outline). (c) ADC map ( $2400/81$ ;  $b = 800 \text{ sec/mm}^2$ ) shows restriction at the suspicious region in the left peripheral zone (outlined), indicating intermediate to highly aggressive tumor. Analysis of MR-guided

biopsy specimen from the suspicious lesion resulted in Gleason score of 8 (3+5) in 80% of the specimen volume, with extension into periprostatic fat (stage T3a).

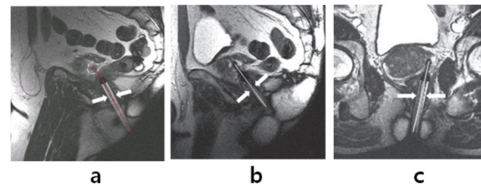


Figure 17. (a, b) Sagittal and (c) axial gradient-echo MR images ( $4.48/2.24$ ; flip angle,  $70^\circ$ ) of MR-guided biopsy in a case of active surveillance of prostate cancer in a 69-year old man (same patient as in Figure 16) with Gleason score 6 (3+3) disease. Multiparametric staging MR imaging (not shown) with an endorectal coil resulted in suspicion of stage T3A cancer in left peripheral zone at midprostate. DW imaging (not shown) findings indicated intermediate to highly aggressive tumor in left peripheral zone<sup>[38]</sup>.

Figure 17 (a) is needle guide (arrows) is positioned toward target in left peripheral zone at midprostate (outline). To accurately hit the target, the needle guide should be moved slightly caudad in sagittal plane; in position shown (red line), the needle will miss the target. (b, c) Needle guide (arrows) is now accurately positioned and biopsy needle (line) has been inserted. MR guided biopsy of this suspicious lesion resulted in a Gleason score of 8 (3+5) for a volume percentage of 80% with extension into periprostatic fat (stage T3A). This patient was subsequently excluded from the active surveillance protocol.

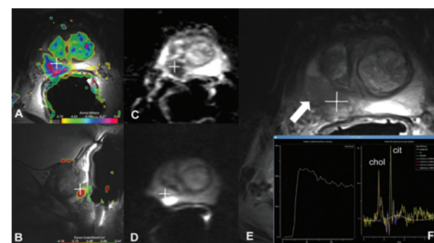


Figure 18. Multiparametric MR imaging of the prostate in screenshot generated by a computer-program, which can be used for image interpretation

in multiparametric MR imaging<sup>[38]</sup>.

Figure 18 is to related views of multiplanar multiparametric images (A–E), and quantitative information (F) is also displayed. A–E show tumor with bulging, suspicious for minimal stage T3A disease, in right peripheral zone at level of midprostate to apex (arrow). A, Axial Ktrans map from dynamic contrast-enhanced MR imaging projected over T2-weighted image. B, Sagittal T2-weighted image (4290/98; flip angle, 120°) with color overlay showing washout (from dynamic contrast-enhanced MR imaging). C, Axial ADC map (2900/81; flip angle, 90°). D, Axial DW trace image (b = 800 sec/mm<sup>2</sup>; 2900/81; flip angle, 90°). E, Axial T2-weighted image. F, Relative gadolinium concentration–time curve (left) and MR spectrum (right) from chosen point of interest in tumor (+). In MR spectrum, choline (chol) and citrate (cit) peaks can be evaluated. The low-signal-intensity lesion on E shows increased Ktrans (on A), restriction on C, high signal intensity on D, gadolinium concentration–time curve type 3 and high choline peak on F. On a five-point scale, this can be scored 5/5 on T2-w, dynamic contrast-enhanced, DW, and MR spectroscopic images, for total score of 20/20, indicating intermediate to highly aggressive tumor<sup>[38]</sup>.

## 12. Diffusion-weighted imaging in combination with T2-weighted imaging

T2-weighted imaging has been shown to provide some localization information in this setting, with previously reported sensitivities and specificities of 67-81% and 46-69%, respectively. MR spectroscopy has shown promise in prostate cancer localization with a sensitivity of 73% and a specificity of 80%. Diffusion-weighted imaging (DWI) is an MRI method typically used in neuroradiology. From DWI parametric maps, apparent diffusion coefficients

(ADCs) can be calculated. Recently, a number of investigators have reported the potential usefulness of DWI for detecting prostate cancer because it shows a lower ADC than a normal peripheral zone [2, 5-7]. The objective of this study to compare T2-weighted MRI alone and T2 combined with diffusion-weighted imaging (DWI) for the localization of prostate cancer. T2-weighted imaging and DWI (b value = 600 s/mm<sup>2</sup>) were performed before radical prostatectomy using an endorectal coil at 1.5 T in this prospective trial. The peripheral zone of the prostate was divided into sextants and the transition zone into left and right halves. T2 images alone and then T2 images combined with apparent diffusion coefficient (ADC) maps (T2 + DWI) were scored for the likelihood of tumor and were compared with whole-mount histology results. Fixed window and level settings were used to display the ADC maps. Only tumors with an area of more than 0.13 cm<sup>2</sup> (> 4 mm diameter) and a Gleason score of  $\geq 6$  were considered significant. The area under the receiver operating characteristic curve (Az) was used to assess accuracy. In the peripheral zone, the Az value was significantly higher (p = 0.004) for T2 plus DWI (Az = 0.89) than for T2 imaging alone (Az = 0.81). Performance was poorer in the transition zone for both T2 plus DWI (Az = 0.78) and T2 (Az = 0.79). For the whole prostate, sensitivity was significantly higher (p < 0.001) with T2 plus DWI (81% [120/149]) than with T2 imaging alone (54% [81/149]), with T2 plus DWI showing only a slight loss in specificity compared with T2 imaging alone (84% [204/243] vs 91% [222/243], respectively). Combined T2 and DWI MRI is better than T2 imaging alone in the detection of significant cancer (Gleason score  $\geq 6$  and diameter > 4 mm) within the peripheral zone of the prostate<sup>[39]</sup>.

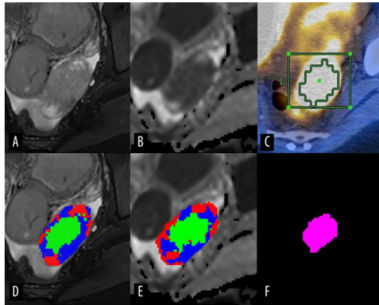


Figure 19. Representative case presenting the combined high-cellularity tumor volume (HCTVC) segmented by both T2-weighted imaging (T2WI) and diffusion-weighted imaging (DWI), as compared with the metabolic tumor volume (MTV) defined in positron emission tomography with computed tomography (PET/CT). (A) T2WI and (D) manually drawn region of interest (ROI), divided into 3 clusters. (B) Apparent diffusion coefficient (ADC) map and (E) manually drawn ROI, divided into 3 clusters. (C) PET/CT and manually drawn ROI, generated by using 45% maximum standard uptake value as the lower threshold. (F) The HCTVC was obtained by excluding low-intensity pixels on T2WI and high ADC pixels on ADC maps.<sup>[39]</sup>

### 13. Dynamic contrast enhanced imaging

Angiogenesis is an integral part of benign prostatic hyperplasia (BPH), is associated with prostatic intraepithelial neoplasia (PIN) and is key to the growth and for metastasis of prostate cancer. Dynamic contrast enhanced magnetic resonance imaging (DCE-MRI) using small molecular weight gadolinium chelates enables non-invasive imaging characterization of tissue vascularity. Depending on the technique used, data reflecting tissue perfusion, microvessel permeability surface area product, and extracellular leakage space can be obtained. Two dynamic MRI techniques (T2\*-weighted or susceptibility based and T1-weighted or relaxivity enhanced methods) for prostate gland evaluations are discussed in this review with reference to biological basis of observations, data acquisition and analysis methods, technical limitations and validation. Established clinical roles of T1-weighted imaging evaluations were discussed including lesion detection

and localization, for tumor staging and for the detection of suspected tumor recurrence. Limitations included inadequate lesion characterization particularly differentiating prostatitis from cancer, and in distinguishing between BPH and central gland tumors<sup>[40]</sup>. DCE-MRI techniques utilising low molecular weight contrast media have become mainstream clinical tools with recognised indications in the imaging of prostate cancer. Current roles of T1-weighted techniques include tumour staging (depiction of capsular penetration and seminal vesicle invasion) and for the detection of suspected tumour recurrence following definitive treatment. Its exact role in monitoring tumour response to hormonal treatment and radiation remains to be defined although its<sup>[40]</sup>.

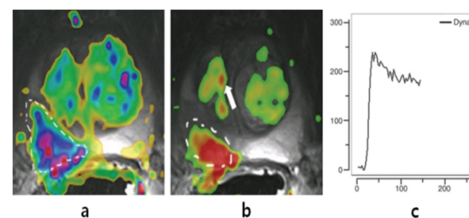


Figure 20. Dynamic contrast-enhanced MR imaging of prostate cancer in 65-year-old man with PSA level of 8.3 ng/mL, clinical stage T2c cancer, and Gleason score of 7 (3+4) in 80% of the volume of systematic random biopsy specimens<sup>[38]</sup>.

Figure 20 (a) is a right peripheral zone (outline) shows contrast enhancement (red) that is suspicious for prostate cancer. (b) in addition to the transition zone (arrow), right peripheral zone (outline) shows increased washout. (c) is relative gadolinium concentration (y-axis)-time (x-axis) curve of tumor shows a type 3 curve with fast increase, fast time to peak, and washout, which are suspicious for cancer.

### 15. MR imaging and MR Spectroscopic imaging

Magnetic resonance imaging (MRI) and proton

magnetic resonance spectroscopy (1H MRSI) are emerging as the most sensitive tools for noninvasive, anatomical and metabolic evaluation of prostate cancer. This article reviews the current applications of MRI and 1H MRSI in clinical practice and discusses the potential of these modalities for improving prostate cancer management. MRI shows zonal anatomy with excellent contrast resolution and can reveal tumors in areas not routinely sampled on biopsies and not palpable on digital rectal exams. MR imaging also allows evaluation of local extent (including extracapsular extension and seminal vesicle involvement), providing surgeons and radiotherapists with a visual roadmap for treatment planning while supporting local staging. Adding 1H MRSI to MRI can improve prostate cancer detection and tumor volume evaluation. It also indirectly contributes to improving local staging. Additionally, 1H MRSI metabolic and volumetric data correlate with pathological Gleason grade and thus may provide a non-invasive means to better predict prostate cancer aggressiveness. Combined MRI/1H MRSI currently has the greatest value for high-risk patients. With a greater understanding of the relationship between spectroscopic data and tumor biology, MRI/1H MRSI can be used to achieve more accurate stratification of patients in clinical trials and monitor patient progress in choosing watchful waiting or minimally aggressive cancer therapies. monitoring may be possible<sup>[41]</sup>.

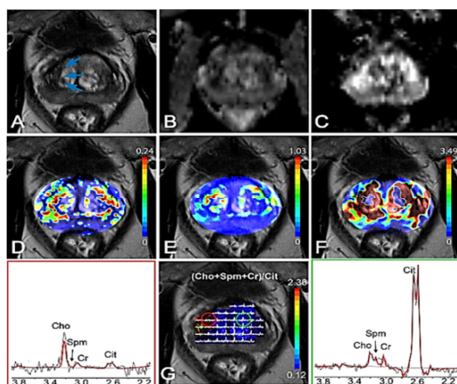


Figure 21. Multiparametric MRI of the prostate of a 58-year-old man with an elevated serum PSA level of 6.8 ng/mL and cancer-negative biopsy results.

**A** T2WI with low-signal intensity areas in the left and right transition zone (arrows) which were biopsy negative for cancer. **B** ADC map showing low-signal intensity for the same areas. High-signal intensity for these areas were seen on **C** high b-value DWI and on pharmacokinetic maps of **D**  $K^{trans}$ , **E**  $K_{ep}$ , and **F** iAUGC. **G** Middle: MRSI grid and color-coded map overlaid on T2WI. The spectra in the yellow box at the right side and in the green box at the left side represent voxels from histopathology confirmed normal tissue (circles)

## 16. PET imaging

Prostate-specific membrane antigen (PSMA) is a cell surface enzyme highly expressed in prostate cancer (PCa) and is currently being extensively explored as a promising target for molecular imaging in various clinical situations. New antibodies and small molecule PSMA radiotracers labeled with various radionuclides for positron emission tomography (PET) imaging applications have been developed and explored in recent studies. Much progress has been made in defining the clinical usefulness of this class of PET formulations, primarily through small-scale and retrospective clinical studies. The strongest data to date are in the setting of biochemically recurrent PCa, where PSMA-targeted radiotracers have been shown to be superior to conventional imaging and other molecular imaging agents for the detection of locally recurrent and metastatic PCa. However, early data suggest that although intraoperative guidance may still be promising, initial lymph node staging before definitive treatment may be limited in high-risk primary PCa patients. Other examples of potential promising applications for PSMA PET imaging include non-invasive characterization of primary PCa, staging and treatment planning for PSMA-targeted radiotherapy, and focal treatment guidance for oligometastatic disease. However, all these indications and applications for PCa PSMA PET imaging are still lacking and large-scale

prospective and systematic clinical trials are needed for validation. As the fields of molecular imaging, urology, radiation oncology, and medical oncology continue to define and refine the usefulness of PSMA-targeted PET imaging to improve the management of PCa patients, such validation trials are needed and hopefully soon<sup>[42]</sup>.

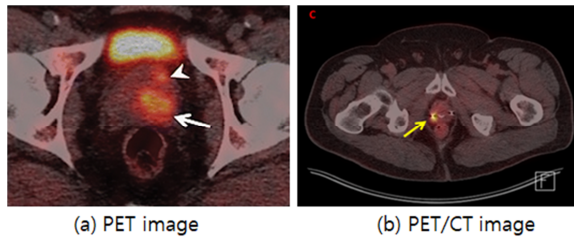


Figure 22. PET and PET/CT images for Prostate cancer detection<sup>[43]</sup>

#### IV. Discussion

An ultrasound guided prostate biopsy is a procedure where a special needle is inserted into the prostate gland to take a small sample of tissue from the gland<sup>[44]</sup>. The sample is then sent to a laboratory for testing, to determine the presence or absence of prostate cancer. MRI scanner uses strong magnetic fields to create an image of the prostate and surrounding tissues. MRI is generally requested because it provides more detailed images of the prostate gland than other radiological tests, such as computed tomography (CT) or ultrasound<sup>[45]</sup>. Sometimes image-guided or surgical biopsy may be required to confirm or exclude disease activity in areas of concern seen on PET imaging<sup>[46]</sup>. The advantages of detection and biopsy of prostate cancer by fusion image guidance are as follows<sup>[47]</sup>. This technique allows specialists to find hidden tumors that may be missed by other prostate biopsies. We can perform targeted biopsies using sophisticated MRI/ultrasound fused images to focus on the worrisome areas directly. The technology, which has

proven to be very useful for men with previous negative biopsies, may also help detect aggressive cancers in patients who have not had a previous biopsy. It may reduce the number of biopsies you need. Although imaging modalities for prostate cancer vary, transrectal ultrasound (TRUS)-guided biopsy remains the standard for diagnosis. However, TRUS has low sensitivity, resulting in a high rate of false negative results. MRI currently provides the most accurate image-based assessment of the prostate. Therefore, TRUS/MRI fusion image-guided biopsy has evolved as the method of choice to overcome the limitations of TRUS-only biopsy. Most frameworks providing these solutions rely on strict TRUS/MRI fusion and make little use of additional information from other modalities such as PET. This is because other frameworks require long interaction times and are complex to integrate with clinical workflows<sup>[48]</sup>. There is currently no clinical workflow that can fully meet the clinical requirements of speed and high precision simultaneously at low cost<sup>[48]</sup>. The development of an open-source fusion biopsy framework that is low-cost, easy-to-use, and has minimal overhead in the clinical workflow seems necessary<sup>[48]</sup>. This will require the implementation of new image registration and visualization approaches and the establishment of a research platform for rapid bench-to-bedside conversion.

#### V. Conclusion

A risk factor directly associated with developing prostate cancer is age. Prostate cancer is very rare under the age of 40 and increases rapidly with age after age 50. The clinical management of prostate cancer is one of the most controversial areas in medicine, with no consensus on the need for cancer screening, the choice of diagnostic tests for pretreatment evaluation, and the need and

appropriateness of treatment for all stages of the disease. Currently, the only sure way to confirm prostate cancer is through a prostate biopsy. Rapid technological advances over the past few years have enabled the mainstream use of prostate imaging for the clinical management of prostate cancer. In biopsy for the diagnosis of prostate cancer, prostate imaging technology is mobilized to extract tissue from the exact area. Ultrasound imaging, MRI, and PET imaging methods are used for prostate imaging methods. Although each image has its own characteristics, the recent trend is the fusion image method that uses each other's strengths. There is currently no technology that can fully meet the clinical requirements of speed and high precision at the same time at low cost. The development of a biopsy framework that is inexpensive, easy to use, and has minimal clinical overhead seems necessary. This requires the implementation of new image registration and visualization approaches and the establishment of a research platform for rapid bench-to-bed conversion.

### Competing interests

The authors declare that there are no competing interests.

### [Reference]

- [1] H. Lilja, “*Structure and function of prostatic- and seminal vesicle-secreted proteins involved in the gelation and liquefaction of human semen*”, Scand J Clin Lab Invest Suppl (1988) Vol. 191, PP. 13-20. <https://doi.org/10.1172/JCI113070>
- [2] [8794.00.pdf \(cancer.org\)](https://pubmed.ncbi.nlm.nih.gov/879400/)
- [3] Ian M. Thompson, Donna P. Ankerst, “*Prostate-specific antigen in the early detection of prostate cancer*”, CMAJ (2007) Vol. 176, PP. 1853-1858. <https://doi.org/10.1503/cmaj.060955>
- [4] Jean-Luc Descotes, “*Diagnosis of prostate cancer*”, Asian Journal of Urology (2018) Vol. 6, PP.



- 129-136. <https://doi.org/10.1016/j.ajur.2018.11.007>
- [5] Samir S. Taneja, “*Prostate Biopsy: Targeting Cancer for Detection and Therapy*”, Rev Urol. (2006) Vol. 8, PP. 173-182. PMID: [17192796](https://pubmed.ncbi.nlm.nih.gov/17192796/)
- [6] Masatomo Kaneko, Maria Sarah L. Lenon, Lorenzo Storino Ramacciotti, et al., “*Multiparametric ultrasound of prostate: role in prostate cancer diagnosis*”, Therapeutic Advances in Urology (2022) Vol. 14, 17562872221145625. PMID: [36601020](https://pubmed.ncbi.nlm.nih.gov/36601020/)
- [7] Sanjay Sharma, “*Imaging and intervention in prostate cancer: Current perspectives and future trends*”, Indian J Radiol Imaging (2014) Vol. 24, PP. 139-148. <https://doi.org/10.4103/0971-3026.134399>
- [8] Kazuhiro Kitajima, Robert C Murphy, Mark A Nathan, et al, “*Update on positron emission tomography for imaging of prostate cancer*”, International Journal of Urology (2014) Vol. 21, PP. 12–23. <https://doi.org/10.1111/iju.12250>
- [9] [Prostate Gland \(Human Anatomy\): Prostate Picture, Definition, Function, Conditions, Tests, and Treatments \(webmd.com\)](https://www.ncbi.nlm.nih.gov/pubmed/23421411)
- [10] Young Barbara, O’Dowd Geraldine, Woodford Philip, “*Wheater’s functional histology: a text and colour atlas (6th ed.)*”, Elsevier (2013) PP. 347-348. [ISBN 9780702047473](https://doi.org/10.1016/B978-0-7020-4747-3).
- [11] Leissner KH, Tisell LE, “*The weight of the human prostate*”. Scand. J. Urol. Nephrol. (1997) Vol. 13, PP. 137-142. <https://doi.org/10.3109/00365597909181168>.
- [12] <https://en.wikipedia.org/wiki/Prostate>
- [13] “*Prostate Gland Development*”. ana.ed.ac.uk. Archived from [the original](#) on 2003-04-30. Retrieved 2011-08-03.
- [14] Standing Susan, “*Prostate*”. *Gray’s anatomy: the anatomical basis of clinical practice (41st ed.)*, Philadelphia. pp. 1266–1270.
- [15] <https://www.cancer.org/cancer/prostate-cancer/about/what-is-prostate-cancer.html>
- [16] R. R. Raylman, S. Majewski, S. K. Lemieux, et al., “*Simultaneous MRI and PET imaging of a rat brain*” Phys. Med. Biol. (2006) Vol. 51, PP. 6371–6379. <https://doi.org/10.1088/0031-9155/51/24/006>
- [17] Hengli Yang, Wenbin Cai, Lei Xu, et al, “*Nanobubble–Affibody: Novel ultrasound contrast agents for targeted molecular ultrasound imaging*

*of tumor*”, *Biomaterials* (2015) Vol. 37, PP. 279-288.  
<https://doi.org/10.1016/j.biomaterials.2014.10.013>

[18] Hak Jong Lee, Young Il Yoon, Yun Jung Bae, “*Theranostic ultrasound using microbubbles in the treatment of prostate cancer*”, *Ultrasonography* (2016) Vol. 35, PP. 309-317.  
<http://dx.doi.org/10.14366/usg.16006>

[19] Rogier R. Wildeboer, Ruud J.G. van Sloun, Arnoud W. Postema, et al., “*Accurate validation of ultrasound imaging of prostate cancer: a review of challenges in registration of imaging and Histopathology*”, *Journal of Ultrasound* (2018) Vol. 21, PP. 197–207. <https://doi.org/10.1007/s40477-018-0311-8>

[20] T.Loch, T. Gettys, J.S. Cochran, et al., “*Computer-aided image analysis in transrectal ultrasound of the prostate*”, *World Journal of Urology* (1990) Vol. 8, PP. 150-153

[21] Lucy A. M. Simmons, Philippe Autier, Frantisek Zatura, et al., “*Detection, localisation and characterisation of prostate cancer by Prostate HistoScanning*”, *BJU International* (2011)

<https://doi.org/10.1111/j.1464-410X.2011.10734.x>

[22] Georg Salomon, Jan Spethmann, Ann Beckmann, et al., “*Accuracy of HistoScanning™ for the prediction of a negative surgical margin in patients undergoing radical prostatectomy*”, *BJUI* (2013) Vol. 111, PP. 60-66.  
<https://doi.org/10.1111/j.1464-10X.2012.11396.x>

[23] Martha K.Terris Thomas A.Stamey, “*Determination of Prostate Volume by Transrectal Ultrasound*”, *The Journal of Urology*, Vol. 145, PP. 984-987.  
[https://doi.org/10.1016/S0022-5347\(17\)38508-7](https://doi.org/10.1016/S0022-5347(17)38508-7)

[24] I. M. Kelly, W. R. Lees, D. Rickards, “*Prostate cancer and the role of color Doppler US*”, *Radiology* (1993) Vol. 189, No. 1,  
<https://doi.org/10.1148/radiology.189.1.7690489>

[25] Michael Mitterberger, Wolfgang Horninger, Friedrich Aigner, “*Ultrasound of the prostate*”, *Cancer Imaging Society* (2010) Vol. 10, PP. 40-48.  
<https://doi.org/10.1102/1470-7330.2010.0004>

[26] Ethan J. Halpen, “*Contrast-Enhanced Ultrasound Imaging of Prostate Cancer*”, *Rev Urol* (2006) Vol. 8, PP. S29-S37. PMID: [17021624](https://pubmed.ncbi.nlm.nih.gov/17021624/)

[27] W. F. Dähnert, U. M. Hamper, J. C. Eggleston, “*Prostatic evaluation by transrectal sonography*

*with histopathologic correlation: the echopenic appearance of early carcinoma*”, *Radiology* (1986) vol. 158, no. 1, pp. 97–102, View at: [Google Scholar](#)

[28] F. Gómez Veiga, J. Ponce Reixa, A. Barbagelata López, et al., “*Current role of PSA and other markers in the diagnosis of prostate cancer*”, *Archivos Espanoles de Urologia* (2006) vol. 59, PP. 1069–1082, View at: [Google Scholar](#)

[29] T. Borza, R. Konijeti, and A. S. Kibel, “*Early detection, PSA screening, and management of over-diagnosis*” *Hematology/Oncology Clinics of North America* (2013) vol. 27, PP. 1091–1110, 2013. View at: [Publisher Site](#) | [Google Scholar](#)

[30] J. Kurhanewicz, D. Vigneron, P. Carroll, and F. Coakley, “*Multiparametric magnetic resonance imaging in prostate cancer: present and future*”, *Current Opinion in Urology*, vol. 18, PP. 71–77, View at: [Publisher Site](#) | [Google Scholar](#)

[31] D. Junker, T. De Zordo, M. Quentin, M. Ladurner et al., “*Real-Time Elastography of the Prostate*”, *BioMed Research International* (2014) Volume 2014, ID 180804  
<https://doi.org/10.1155/2014/180804>

[32] Qi Ma, Dong-Rong Yang, Bo-Xin Xue, et al., “*Transrectal real-time tissue elastography targeted biopsy coupled with peak strain index improves the detection of clinically important prostate cancer*”, *Oncology Letters* (2017) Vol. 14, PP. 210-216. <https://doi.org/10.3892/ol.2017.612>

[33] Shuai Fu, Yuzhe Tang, Shi Tan, et al., “*Diagnostic Value of Transrectal Shear Wave Elastography for Prostate Cancer Detection in Peripheral Zone: Comparison with Magnetic Resonance Imaging*”, *Journal of Endourology* (2019) Vol. 34. No. 5,  
<https://doi.org/10.1089/end.2019.0902>

[34] Liang Zhai, John Madden, Wen-Chi Foo et al., “*Acoustic Radiation Force Impulse Imaging of Human Prostates Ex Vivo*”, *Ultrasound of Medicine & Biology* (2010) Vol. 36, PP. 576-588.  
<https://doi.org/10.1016/j.ultrasmedbio.2009.12.006>

[35] Mark L. Palmeri, Kathryn R. Noghtingale, “*Acoustic radiation force-based elasticity imaging methods*”, *Interface Focus* (2011) Vol. 1, No. 4,  
<https://doi.org/10.1098/rsfs.2011.0023>

[36] Arash Maghsoudi, Mehran Jahed, “*Multi-*

*parameter sensitivity analysis for guided needle insertion through soft tissue*", IEEE EMBS Conference on Biomedical Engineering and Sciences(IECBES) (2010)

IBSPEC Accession Number: 11910631

<https://doi.org/10.1109/IECBES.2010.5742207>

[37] Yushan Liu, Shi Zeng, Ran Xu, "*Application of Multiple Ultrasonic Techniques in the Diagnosis of Prostate Cancer*", Front. Oncol., (2022) Sec. Cancer Imaging and Image-directed Interventions, <https://doi.org/10.3389/fonc.2022.905087>

[38] Caroline M. A. Hoeks, Jelle O. Barentsz, Thomas Hambroek, et al., "*Prostate Cancer: Multiparametric MR Imaging for Detection, Localization, and Staging*", Radiology (2011) Vol. 261, No. 1, PP. 46-66.

[39] Qing Wu, Xiufang Xu, "*Combining Diffusion-Weighted Imaging and T2-Weighted Imaging to Delineate Tumorous Tissue in Peritoneal Carcinomatosis: A Comparative Study with 18F-Fluoro-Deoxyglucose Positron Emission Tomography with Computed Tomography (FDG PET/CT)*", Medical Science Monitor (2022) Vol. 28, e934664 <https://doi.org/10.12659/MSM.934664>

[40] Roberto Alonzi, Anwar R. Padhani, Clare Allen, "*Dynamic contrast enhanced MRI in prostate cancer*", European Journal of Radiology (2007) Vol. 63, PP. 335-350.

<https://doi.org/10.1016/j.ejrad.2007.06.028>

[41] H. Hricak, "*MR imaging and MR spectroscopic imaging in the pre-treatment evaluation of prostate cancer*", BJR (2014)

<https://doi.org/10.1259/bjr/11253478>

[42] S. P. Rowe. M. A. Gorin, M. E. Allaf, et al., "*PET imaging of prostate-specific membrane antigen in prostate cancer: current state of the art and future challenges*", Prostate Cancer and Prostatic Diseases (2016) Vol. 19, PP. 223-230.

<https://doi.org/10.1038/pcan.2016.13>

[43] Jody A. Charnow, "*PET/CT Imaging for Recurrent PCa Detection More Accurate With PSMA*", Cancer Therapy Advisor (2019) The American Society of Clinical Oncology 2019 meeting

<https://www.cancertherapyadvisor.com/home/cancer-topics/prostate-cancer/pet-ct-imaging-for-recurrent-pca-detection-more-accurate-with-psma/>

[44] <https://www.insideradiology.com.au/ultrasound-guided-prostate-biopsy/>

[45] Tobias Penzkofer, Clare M. Tempny-Afdha, "*Prostate Cancer Detection and Diagnosis: The Role of MR and its Comparison to other Diagnostic Modalities – A Radiologist's Perspective*", NMR Biomed (2013) Vol. 27 Total page 27.

<https://doi.org/10.1002/nbm.3002>

[46] Renjith Kalathoorakathu Radhakrishnan, Bhagwant Rai Mittal, Arun Kumar Reddy Gorla, et al, "*Real-time intraprocedural <sup>18</sup>F-FDG PET/CT-guided biopsy using automated robotics arm (ARA) in the diagnostic evaluation of thoracic lesions with prior inconclusive biopsy results*", Br J Radiol (2017) Vol. 90, Total page 11

<https://doi.org/10.1259/bjr.20170258>

[47] Sunao Shoji, "*Magnetic resonance imaging-transrectal ultrasound fusion image-guided prostate biopsy: Current status of the cancer detection and the prospects of tailor-made medicine of the prostate cancer*", Investig Clin Urol (2019) Vol. 60, PP. 4-13.

<https://doi.org/10.4111/icu.2019.60.1.4>

[48] Mostafa A. Arafa, Danny M. Rabah, Farruhk K. Khan, et al., "*Effectiveness of magnetic resonance imaging-targeted biopsy for detection of prostate cancer in comparison with systematic biopsy in our countries with low prevalence of prostate cancer*", Prostate Int. (2021) Vol. 9, PP. 140-144.

<https://doi.org/10.1016/j.pmil.2021.01.001>